


[View Journal Online](#)
[View Article Online](#)

Joule-Thomson coefficients and inversion curves from newly developed cubic equations of state

 Binay Prakash Akhouri ^{1,*} and Sumit Kaur ²
¹ Department of Physics, Birsa College, Khunti-835210, Jharkhand, India
binayakhouri@yahoo.in (B.P.A.)

² Department of Physics, Nirmala College, Ranchi-834002, Jharkhand, India
sumitbharaj@gmail.com (S.K.)

 * Corresponding author at: Department of Physics, Birsa College, Khunti-835210, Jharkhand, India.
 Tel: +99.0651.2205177 Fax: +99.0651.2214077 e-mail: binayakhouri@yahoo.in (B.P. Akhouri).

RESEARCH ARTICLE

ABSTRACT



doi 10.5155/eurjchem.10.3.244-255.1883

 Received: 23 April 2019
 Received in revised form: 02 July 2019
 Accepted: 09 July 2019
 Published online: 30 September 2019
 Printed: 30 September 2019

KEYWORDS

 Uncertainty
 Equations of state
 Cohesion functions
 Newton Raphson method
 Joule-Thomson coefficients
 Joule Thomson inversion curves

In this work, we have generalized different parametric forms of cubic equations of state (EoSs) to predict complete Joule-Thomson (J-T) inversion curves for methane at wide temperature and pressure ranges. EoSs of the Soave-Redlich-Kwong (SRK), Peng-Robinson (PR), Patel-Teja (PT), Esmailzadeh-Roshanfeker (ER) and the Hagtalah-Kamali-Mazloumi-Mahmoodi (HKMM) along with frequently used cohesion functions $\alpha(T_r)$ have been considered for plot of J-T inversion curves. The PR EoS along with different cohesion functions such as those of the Soave, Antonin Chapoy and the Tau-Sim-Tassone have been also tested for accurate prediction of the inversion curves. The four parametric EoSs of Adachi-Lu-Sugie (ALS), and Lawal-Lake-Silberberg (LLS) with their associated cohesion functions have been used for the prediction of J-T inversion curves. It has been observed that for the plot of inversion curves the LLS EoS is inadequate while the ER EoS agrees well with the previous measurements made in Laboratory. Besides, the J-T coefficient measurements from EoSs have been made for carbon dioxide and nitrogen gases at temperatures from 273.15 to 473.15 K and at pressures from 10 to 1000 atm, respectively. The uncertainties of experimental J-T coefficients data of carbon dioxide from values calculated using EoSs at constant pressure of 1 atm and 20 atm and with varying temperatures have been studied.

 Cite this: *Eur. J. Chem.* 2019, 10(3), 244-255

 Journal website: www.eurjchem.com

1. Introduction

In between the years 1852 and 1862, J-T effect was discovered and was named after the physicists James Presscot Joule (1818-1889) and William Thomson (1824-1907). They performed the porous plug experiment to study the change of temperature with change of pressure of a gas at constant enthalpy. Roebuck and co-workers [1] and Sage and co-workers [2] studied the J-T effect experimentally and obtained J-T coefficients for inorganic gases and organic compounds. The theoretical prediction of J-T inversion curve is well known as an extremely severe test of an EoS. The J-T inversion curves for the van der Waals, Dieterici, Lennard-Jones, Devonshire and the DeBoer-Michels EoS were plotted before 1970 [3]. The J-T inversion curves for pure components have been calculated by many authors using various cubic EoS [3-10]. Prausnitz *et al.* [11] reviewed many types of EoSs and stated "cubic EoSs have often been chosen as the optimal forms because the accuracy is adequate and the analytic solution for the phase density is not too demanding." Potter [12] has given a brief summary of J-T studies. Nichita *et al.* [13] has also given an account of J-T inversion curve calculations. At considerable range of temperature and pressure, Coleman and Steward [14]

and Bender [15] developed their EoSs to predict the J-T coefficients for fluids such as nitrogen, methane, carbon dioxide etc. Brown [16] has named the J-T inversion curve as Charles curve and is a best criterion for evaluating an EoS for wide ranges of temperature and pressure [17,18]. The critical properties, acentric factor and molecular weight of components are required for calculations as parameter input in EoSs.

The border of Joule-Thomson inversion curve separates the heating region with cooling region. In case of van der Waals EoS, at low temperatures, when, $T \rightarrow 0$, $\mu_{J-T} \approx 2a / RTC_p > 0$ as each term contained therein is a positive and therefore cooling result. At high temperatures, when, $T \rightarrow \infty$, $\mu_{J-T} \approx -b / C_p < 0$, therefore warming results. It has been stated that the Redlich-Kwong (RK) EoS provides best fit among equations of state and found better than the more complex EoSs [19-21]. Dally and Heidmann [22] predicted the J-T inversion curve using four EoSs. The four EoSs were the SRK, PR, Perturbed-Hard-Chain (PHC), and Lee-Kesler (LK). They observed that the studied EoSs give good predictions of the low-temperature branch of the inversion

curve. The high temperature branch and the peak of the inversion curve proved to be sensitive to the EoS parameters and yield poor results. Colina *et al.* [23] simulated the J-T inversion curve for carbon dioxide using two different approaches based on Monte Carlo simulation for the isothermal-isobaric ensemble. The plot of J-T inversion curve appears parabolic in shape, with a maximum inversion pressure at an intermediate temperature. Its volume~temperature plot shows an exponential behavior and the volume approaches infinite limit at extremities of temperature. In this work various EoSs belonging to any of the generalized form has been taken to test the prediction of J-T inversion curves. The J-T inversion curve for newly developed three parameters [24-26] and four parameters [27,28] cubic EoSs have been predicted and compared with the two parameters [29] cubic EoS of PR. Two parameters EoSs such as the SRK EoS, PR EoS and the three parameters EoSs of the PT EoS, ER EoS and the HKMM EoS have been considered [21,24-28]. The four parameters EoSs of LLS EoS and ALS EoS are also considered for predicting the inversion curves.

1.1. The J-T coefficient

The J-T coefficient is a thermodynamic quantity which can be used to increase the understanding of intermolecular force [30-33] between the molecules. To interpret the J-T coefficient in terms of molecular properties, it is assumed that there is no exchange of either heat or work with the surroundings, thus allowing one to use the principle of conservation of energy. The internal energy of the gas is made up of two parts: the kinetic energy of the molecules, depending only on the temperature, and the potential energy, which depends on how far apart they are that is on the expansion of the gas. The expansion of the gas has two alternative effects within itself. First, because of expansion, the average distance between molecules increases resulting in increase of intermolecular attractive forces and hence the increase in potential energy. Therefore, increase in potential energy forces a decrease in kinetic energy and thereby the gas cools down. Secondly, the gas expansion reduces the frequency of molecular collision resulting in a decrease in the average kinetic energy and therefore temperature of gas decreases. For real gas, in adiabatic process, the free expansion (throttling process) occurs not with constant internal energy but with constant heat content (isenthalpic process) or enthalpy H [30]. The Joule-Thomson coefficient μ_{J-T} is therefore defined as the rate of change of temperature with pressure in an isenthalpic expansion. Mathematically, it is written as:

$$\mu_{J-T} = \left(\frac{\partial T}{\partial P} \right)_H \quad (1)$$

In terms of compressibility factor, one may use,

$$\mu_{J-T} = \left(\frac{\partial Z}{\partial T} \right)_P \quad (2)$$

At low and intermediate ranges of temperature and pressure, The J-T coefficients μ_{J-T} have been found usually positive, meaning thereby that a decrease in pressure results in decrease in temperature. But, at high pressure and temperature ranges, the J-T coefficients μ_{J-T} have been found usually negative, meaning thereby that the fluid warms up instead of cooling down after expansion. In case of the free expansion of real gas, we find $H = U + Pv$ is a constant. Therefore, $dH = d(U + Pv) = 0$, if $H = H(T, P)$, then

$$dH = \left(\frac{\partial H}{\partial T} \right)_P dT + \left(\frac{\partial H}{\partial P} \right)_T dP \quad (3)$$

$$\frac{dT}{dP} = - \frac{\left(\frac{\partial H}{\partial P} \right)_T}{\left(\frac{\partial H}{\partial T} \right)_P} = - \frac{\left(\frac{\partial H}{\partial P} \right)_T}{C_p} \quad (4)$$

Here, C_p is a definite numerical quantity and therefore the magnitude of the J-T coefficient is determined mainly by the variation in the quantity H with pressure at constant temperature T . Using relation $dU = TdS - PdV$, and the Maxwell relation $\left(\frac{\partial S}{\partial P} \right)_T = \left(\frac{\partial V}{\partial T} \right)_P$, we can obtain the expression for J-T coefficient as:

$$\mu_{J-T} = \frac{1}{C_p} \left[T \left(\frac{\partial V}{\partial T} \right)_P - V \right] \quad (5)$$

For an ideal gas, $\mu_{J-T} = 0$, thus the temperature of the gas does not change. However, even for non-ideal gas, $\mu_{J-T} = 0$, provided that

$$T \left(\frac{\partial V}{\partial T} \right)_P = V \quad (6)$$

Equation (6) defines a curve in the $T - P$ plane, this curve is known as inversion curve. The isenthalps are curves of constant enthalpy, $H(P, T) = \text{constant}$. The region inside the inversion curve, T increases with P along isenthalps and therefore $\mu_{J-T} = \left(\frac{\partial T}{\partial P} \right)_H > 0$ meaning thereby that gas cools in expansion, while in outside region along the isenthalps it decreases. Therefore, in outside region $\mu_{J-T} = \left(\frac{\partial T}{\partial P} \right)_H < 0$ meaning thereby that gas warms up in expansion. Above the inversion temperature, collision frequency rises with the increase of molecular movement and therefore the gas outside the inversion curve always warms up in Joule-Thomson expansion.

In Section 2, the three generalized forms of attractive terms have been proposed with keeping the van der Waals repulsive term for the EoSs, and corresponding derivatives of compressibility factors with temperatures (at constant pressures) have been expressed in generalized form. These derivatives have been evaluated while calculating the J-T coefficients. In Section 3, a necessary theory for the calculations of J-T inversion curves from the EoSs is given. This section also includes the cohesion functions and its derivatives. Section 4 consists of results and discussion. Finally Section 5 represents the conclusion.

2. The three generalized forms of cubic EoSs

Considering the generalized form of cubic EoSs [20-26] as:

$$P = \frac{RT}{v-b} - \frac{a}{(v+nX)(v+mY)} \quad (7)$$

where, $a(T)$ is a function of critical temperature, critical pressure and acentric factor.

Table 1. The expressions of Ω_a , Ω_{ac} for ALS and of Ω_a , Ω_b for LLS EoSs*.

ALS EoS	LLS EoS
$\Omega_a = \Omega_{ac} (1 + m(1 - T_r^{0.5}))^2$	$\Omega_a = (1 + (\Omega_w - 1)Z_c)^3$
$\Omega_{ac} = 0.44869 + 0.04024\omega + 0.01111$	$\Omega_b = \Omega_w Z_c$
$m = 0.4070 + 1.3787\omega - 0.2933\omega^3$	

* The available value for SRK EoS, $\Omega_a = 0.4278$, $\Omega_b = 0.0867$; for PR EoS, $\Omega_a = 0.45724$, $\Omega_b = 0.07780$ and for TST EoS, $\Omega_a = 0.470507$, $\Omega_b = 0.0740740$.

Table 2. The calculated values of Ω_a , Ω_b and Ω_c for selected EoSs.

Compound	Acentric factor ω	Patel Teja (PT) Equation of State			Esmailzadeh Roshanfekar (ER) Equation of State			Haghtalab Kamali Mazloumi Mahmoodi (HKMM) Equation of State		
		Ω_a	Ω_b	Ω_c	Ω_a	Ω_b	Ω_c	Ω_a	Ω_b	Ω_c
Methane	0.008	0.43299	0.08494	0.01474	0.43775	0.08718	0.05175	0.458978	0.088579	-0.36249
Ethane	0.098	0.44060	0.08265	0.03487	0.44264	0.08386	0.05930	0.460762	0.086068	-0.37601
Propane	0.152	0.44504	0.08133	0.04643	0.44589	0.08210	0.06385	0.461962	0.084441	-0.38373
n-Butane	0.193	0.44834	0.08036	0.05500	0.44852	0.08088	0.06732	0.462941	0.083148	-0.39207
n-Pentane	0.251	0.45289	0.07904	0.06672	0.45247	0.07932	0.07224	0.464431	0.081235	-0.40278
Hydrogen	0.220	0.41251	0.09136	0.04086	0.42833	0.09781	0.03289	0.455536	0.093761	-0.33535
Oxygen	0.021	0.43410	0.08460	0.01771	0.43841	0.08667	0.05284	0.459220	0.088232	-0.36434
Nitrogen	0.040	0.43573	0.08412	0.02201	0.43941	0.08594	0.05443	0.459583	0.087716	-0.36501
Carbon dioxide	0.225	0.45087	0.07962	0.06152	0.45066	0.07999	0.07003	0.463747	0.082105	-0.39789
Ammonia	0.250	0.45282	0.07906	0.06652	0.45240	0.07934	0.07215	0.464405	0.081269	-0.40259

$$Z_c^3 + (mC + (n-1)B - 1)Z_c^2 + ((nB - B - 1)mC - (B+1)nB + A)Z_c - (nmCB(B+1) + AB) = 0 \quad (8)$$

$$Z_c^3 + ((m+n)C - B - 1)Z_c^2 + (nmC^2 - (n+m)BC - (n+m)C + A)Z_c + (-nmC^2B - nmC^2 - AB) = 0 \quad (9)$$

$$Z_c^3 + ((m+n)B - B - 1)Z_c^2 + (nmB^2 - (n+m)B^2 - (n+m)B + A)Z_c - (nmB^2 + nmB^3 + AB) = 0 \quad (10)$$

In attractive term of Equation (7), the denominator of first parenthesis contains second term as nX and the second parenthesis contains second term as mY . In order to express the three forms of cubic EoSs, we put, $X = b$ and $Y = c$, $X = c$ and $Y = c$, and $X = b$ and $Y = b$ in Equation (7), respectively. The third form (case III) represents the two parameters form of the cubic EoS. In all the three forms, the constant a , b and c of the cubic EoS are given by,

$$a = \Omega_a \frac{R^2 T_c^2}{P_c} \alpha(T); \quad b = \Omega_b \frac{RT_c}{P_c}; \quad c = \Omega_c \frac{RT_c}{P_c}.$$

Table 1 shows the expressions of Ω_a , Ω_{ac} for ALS and of Ω_a , Ω_b for LLS EoSs. The values of these parameters can be determined as a function of pure compound acentric factor value. In Table 1, the critical compressibility factor, Z_c and the van der Waals constant parameter, Ω_w were determined as a function of acentric factor. The calculated values of the parameters Ω_a , Ω_b and Ω_c for selected EoSs are given in Table 2. These calculations were performed by the use of Newton Raphson method and parameters as a function of pure compound acentric factor values.

The different cases which arise from Equation (7) are:

Case I for $X = b$ and $Y = c$, the three parameters a , b and c can be calculated by using the critical properties of the pure components and by rearrangements of Equation (7), we obtain Equation (8).

In this case the constants n and m in Equation (7) have the unique values for a given cubic EoS, for example, if one takes $n = 1$ and $m = 0$, the EoS obtained is the SRK EoS; for $n = 3$ and $m = -0.5$, the TST EoS is obtained, for $n = -0.5$

and $m = -0.5$ the HKMM EoS, $n = 1 + \sqrt{3}$ and $m = 1 - \sqrt{3}$ the NM EoS is obtained.

Case II for $X = c$ and $Y = c$, the three parameters a , b and c can be calculated by using the critical properties of the pure components and by rearrangements of Equation (7), we obtain Equation (9).

In this case the constants n and m in Equation (7) have the unique values for a given cubic EoS, for example, if one takes $n = 0$ and $m = 1$, the EoS obtained is the SRK EoS and for $n = 1 - \sqrt{2}$ and $m = 1 + \sqrt{2}$, the ER EoS is obtained.

Case III for $X = b$ and $Y = b$, the three parameters a , b and c can be calculated by using the critical properties of the pure components and by rearrangements of Equation (7), we can obtain Equation (10).

In this case the constants n and m in Equation (7) have the unique values for a given cubic EoS, for example, if one takes $n = 1$ and $m = 0$, the EoS obtained is the SRK EoS and $n = 1 + \sqrt{2}$ and $m = 1 - \sqrt{2}$ the PR EoS is obtained.

The development of stability criterion requires the three relations between T and T_c , if $T < T_c$, there will be three roots of v , if $T > T_c$, there will be only one root of v corresponding to the gas phase and if $T = T_c$, there will be three equal roots of v . Thus, at $T = T_c$, there are also three equal roots of Z . If we call these \bar{Z}_c , then we can write:

$$(Z_c - \bar{Z}_c)^3 = Z_c^3 - 3\bar{Z}_c Z_c^2 + 3Z_c \bar{Z}_c^2 - \bar{Z}_c^3 = 0 \quad (11)$$

Table 3. Coefficients of Equations (8), (9) and (10).

$i = 1$	$i = 2$	$i = 3$
$\alpha_1 = mC + (n-1)B - 1$	$\alpha_2 = (m+n)C - B - 1$	$\alpha_3 = (m+n)B - B - 1$
$\beta_1 = (nB - B - 1)mC - (B+1)nB + A$	$\beta_2 = nmC^2 - (n+m)BC - (n+m)C + A$	$\beta_3 = mnB^2 - (n+m)B^2 - (n+m)B + A$
$\gamma_1 = -(nmCB(B+1) + AB)$	$\gamma_2 = -nmC^2B - nmC^2 - AB$	$\gamma_3 = -(nmB^2 + nmB^3 + AB)$

$$\Omega_a = 3\bar{Z}_c^2 - nm\Omega_b\Omega_c + (n\Omega_b + m\Omega_c)(\Omega_b + 1) \quad (13)$$

$$\Omega_b^3 + (2 - n^2 + n - 3\bar{Z}_c)\Omega_b^2 + (3\bar{Z}_c^2 + (1+n)(1 - 3\bar{Z}_c))\Omega_b - \bar{Z}_c^3 = 0 \quad (14)$$

$$\Omega_c = \frac{1 - 3\bar{Z}_c + (1-n)\Omega_b}{m} \quad (15)$$

$$\Omega_a = 3\bar{Z}_c^2 - nm\Omega_c^2 + (n+m)\Omega_c(\Omega_b + 1) \quad (16)$$

$$\Omega_c^2((m+n)\Omega_c + 3\bar{Z}_c)nm + (3\bar{Z}_c^2 - nm\Omega_c^2 + (n+m)\Omega_c((m+n)\Omega_c + 3\bar{Z}_c))((m+n)\Omega_c + 3\bar{Z}_c - 1) - \bar{Z}_c^3 = 0 \quad (17)$$

$$\Omega_c = \frac{1 - 3\bar{Z}_c + \Omega_b}{m+n} \quad (18)$$

$$\Omega_a = 3\bar{Z}_c^2 - (nm - (n+m))\Omega_b^2 + (n+m)\Omega_b \quad (19)$$

$$nm\Omega_b^3 + nm\Omega_b^2 + (3\bar{Z}_c^2 - (nm - (n+m)\Omega_b^2 + (n+m)\Omega_b)\Omega_b) - \bar{Z}_c^3 = 0 \quad (20)$$

$$\Omega_b = \frac{1 - 3\bar{Z}_c}{n+m-1} \quad (21)$$

Equation (11) is a requirement equivalent to equation (12).

$$\left(\frac{\partial P}{\partial v}\right)_{T_c} = 0; \left(\frac{\partial^2 P}{\partial v^2}\right)_{T_c} = 0, \text{ and } \frac{P_c v_c}{RT_c} = \bar{Z}_c \quad (12)$$

Based on above equations, we have the following cases relating Ω_a , Ω_b and Ω_c to the empirical parameter \bar{Z}_c , with $\alpha(T_r) = 1$.

Case I Comparing Equation (11) with Equation (8), we obtain the Equations (13), (14) and (15).

Case II Comparing Equation (11) with Equation (9), we obtain the Equations (16), (17) and (18).

Case III Comparing Equation (11) with Equation (10), we obtain the Equations (19), (20) and (21).

In all the three cases the values of Ω_b for pure components have been calculated by using Newton Raphson method. Next, with the known value of Ω_b , the parameters Ω_a and Ω_c can readily be calculated. The Equations (8), (9) and (10) can be written in a cubic polynomial form for the compressibility factor Z_c as:

$$f(Z_c) = Z_c^3 + \alpha_i Z_c^2 + \beta_i Z_c + \gamma_i = 0 \quad (22)$$

For the three cases, the coefficients of Equations (8), (9), (10) comparing with the coefficients of Equation (22) are

given in Table 3. The expression for A, B and C in Table 3 has the form: $A = aP/RT^2$, $B = bP/RT$ and $C = cP/RT$.

In PvT system, only any two parameters are required to know the third parameter via the EoS $f(PvT) = 0$. It is well known that the derivatives of any of these parameter helps to determine the thermodynamic property. The cyclic rule of these derivatives may be written as,

$$\left(\frac{\partial P}{\partial v}\right)_T \left(\frac{\partial T}{\partial P}\right)_v \left(\frac{\partial v}{\partial T}\right)_P = -1 \quad (23)$$

Therefore, once we know two of the three PvT derivatives, the third can readily be calculated from Equation (23). The third derivative of Equation (23) is not easier to calculate since Equation (22) is not clearly explicit in volume or temperature. It is therefore found explicitly using Equation (22).

$$\left(\frac{\partial v}{\partial T}\right)_P = \frac{R}{P} \left[T \left(\frac{\partial Z}{\partial T}\right)_P + Z \right] \quad (24)$$

Now, we can find the change of compressibility factor Z with respect to change in temperature T at constant P for the three cases:

Case I: we can find the derivative (Equations (25)).

For **Case II**, the expression of derivative is Equation (26).

Similarly, we have **Case III** as Equation (27).

$$\left(\frac{\partial Z}{\partial T}\right)_p = \frac{\left(\frac{\partial A}{\partial T}\right)_p [B-Z] + \left(\frac{\partial B}{\partial T}\right)_p [(1-n)Z^2 + ((2B+1)n + (1-n)mC)Z + (2B+1)nmC + A] + \left(\frac{\partial C}{\partial T}\right)_p [(1+B)nmB + (1-Z-nB+B)mZ]}{3Z^2 + (mC + (n-1)B-1)2Z + (nB(mC-B-1) - mC(1+B) + A)} \quad (25)$$

$$\left(\frac{\partial Z}{\partial T}\right)_p = \frac{\left(\frac{\partial A}{\partial T}\right)_p [B-Z] + \left(\frac{\partial B}{\partial T}\right)_p [Z^2 + (n+m)CZ + nmC^2 + A] + \left(\frac{\partial C}{\partial T}\right)_p [(n+m)(BZ + Z - Z^2) + (B+1-Z)2nmC]}{3Z^2 + ((n+m)C - B - 1)2Z - (BC + C)(n+m) + nmC^2 + A} \quad (26)$$

$$\left(\frac{\partial Z}{\partial T}\right)_p = \frac{\left(\frac{\partial A}{\partial T}\right)_p [B-Z] + \left(\frac{\partial B}{\partial T}\right)_p [(1-n-m)Z^2 + (3(n+m) - 2nmB)Z + (2B - 3B^2)nm + A]}{3Z^2 + ((n+m) - B - 1)2Z + ((n+m)B(-2B-1) + nmB^2 + A)} \quad (27)$$

$$\left(\frac{\partial A}{\partial T}\right)_p = \frac{P}{R^2 T^2} \left(\frac{\partial a}{\partial T} - \frac{2a}{T} \right) \quad (28)$$

$$\left(\frac{\partial B}{\partial T}\right)_p = -\frac{bP}{RT^2} \quad (29)$$

$$\left(\frac{\partial C}{\partial T}\right)_p = -\frac{cP}{RT^2} \quad (30)$$

3. Calculation of the J-T coefficients and the J-T inversion curves

We can calculate J-T coefficients in three steps. First, the derivative $\left(\frac{\partial Z}{\partial T}\right)_p$ can be calculated for any of the considered EoS by substituting their numerical m and n values in the corresponding generalized case of EoS. Second, the derivative of $\left(\frac{\partial v}{\partial T}\right)_p$ will be calculated from Equation (24). Finally, the J-T coefficient will be calculated by using Equation (5).

3.1. The J-T inversion curves from cubic EoSs

The inversion condition, $\mu_{J-T} = 0$ is given by the following Equation:

$$T \left(\frac{\partial P}{\partial T} \right)_v + v \left(\frac{\partial P}{\partial v} \right)_T = 0 \quad (31)$$

The generalized cubic equation of state is given by the following relation:

$$P = \frac{RT}{v-b} - \frac{a(T)}{v^2 + ubv + wb^2} \quad (32)$$

The denominator of this equation has the form: $v^2 + ubv + wb^2$, the u and w values of some of the equations

of state are given in Table 4. At low temperatures the interactions between molecules may be significant compared to the thermal energy and therefore the term a becomes important while at high temperatures, however, the term b becomes significant as the thermal energy becomes greater than any interaction. Differentiating Equation (32) with respect to temperature at constant volume and multiplying with T , we have,

$$T \left(\frac{\partial P}{\partial T} \right)_v = \frac{RT}{v-b} - \frac{1}{v^2 + ubv + wb^2} \left(T \frac{da}{dT} \right) \quad (33)$$

Differentiating Equation (32) with respect to volume at constant temperature and multiplying with v , we have,

$$v \left(\frac{\partial P}{\partial v} \right)_T = \frac{-RTv}{(v-b)^2} + \frac{av(2v+ub)}{(v^2 + ubv + wb^2)^2} \quad (34)$$

where

$$a = a(T_c) \alpha \quad (35)$$

Differentiating Equation (35) with respect to temperature and multiplying with T , we have

$$T \left(\frac{\partial a}{\partial T} \right) = a(T_c) T \left(\frac{d\alpha}{dT} \right) = a(T_c) \phi \quad (36)$$

Taking $v/b = x$, and using Equation (31) with a little bit algebra, we can write inversion curve Equation (37).

Table 4. Attractive terms of EoSs with values of u and w .

EoS	Attractive terms	u	w
SRK [25]	$\frac{a(T)}{v(v+b)}$	1	0
PR [29]	$\frac{a(T)}{v(v+b)+b(v-b)}$	2	-1
PT [26]	$\frac{a(T)}{v(v+b)+c(v-b)}$	$\frac{b+c}{b}$	$-\frac{b}{c}$
HKMM [25]	$\frac{a(T)}{v\left(v-\frac{b}{2}\right)+b\left(v-\frac{c}{2}\right)}$	$-\left(\frac{c}{2b}+\frac{1}{2}\right)$	$\frac{c}{4b}$
ER [24]	$\frac{a(T)}{v(v+c)+c(v-b)}$	$\frac{2c}{b}$	$-\frac{c^2}{b^2}$
TST [32]	$\frac{a(T)}{v^2+2.5bv-1.5b^2}$	2.5	-1.5
LLS [28]	$\frac{a(T)}{v^2+ubv-wb^2}$	$\frac{1+(\Omega_w-3)Z_c}{\Omega_w Z_c}$	$-\frac{Z_c^2(\Omega_w-1)^3+2\Omega_w^2 Z_c+\Omega_w(1-3Z_c)}{\Omega_w^2 Z_c}$ $Z_c = \frac{0.293}{1+0.375\omega}$ and $\Omega_w = \frac{b}{v_c}$
ALU [27]	$\frac{a(T)}{(v-b_2)(v+b_3)}$	$\frac{\Omega_{b_3}\Omega_{b_2}+\Omega_{b_3}^2}{\Omega_b^2}$	$-\frac{\Omega_{b_2}\Omega_{b_3}}{\Omega_b^2};$ $\Omega_b = 0.08974 - 0.03452\omega + 0.0033\omega^2,$ $\Omega_{b_2} = 0.03686 + 0.00405\omega - 0.01073\omega^2 + 0.00157\omega^3$ $\Omega_{b_3} = 0.15400 + 0.14122\omega - 0.00272\omega^2 - 0.00484\omega^3$

$$F_1(x^2+ux+w)^2 + F_2x(2x+u)(x-1)^2 + F_3(x-1)^2(x^2+ux+w) = 0 \quad (37)$$

where, $F_1 = \Omega_b T_r$, $F_2 = -\Omega_a \alpha(T_r)$ and $F_3 = \Omega_a \phi$ with $\phi = T \left(\frac{d\alpha(T_r)}{dT} \right)$. From Equation (32) the reduced inversion pressure has the following form:

$$P_r = \frac{T_r}{\Omega_b} \frac{1}{(x-1)} - \frac{\Omega_a \phi}{\Omega_b^2} \frac{1}{(x^2+ux+w)} \quad (38)$$

3.2. Cohesion functions and its first derivatives

A study of the frequently used cohesion functions in the selected EoSs has been performed. These α functions together with EoSs have been used in calculating J-T coefficients and J-T curves. The sole knowledge of an experimental value of the acentric factor (ω) makes it possible to evaluate $\alpha(T_r)$. Mathematical conditions on the α function and its derivatives aimed at ensuring consistent and accurate calculations of thermodynamic properties. The α functions are of two types: generalized and component dependent. For generalized α functions only acentric factor (ω) values of pure compounds are required as input parameter while values of component dependent parameters are required for component α function. The selected α functions and its first derivatives

used in this work are given in Table 5. Table 6 represents the values of the constants L , N and M in the associated α function of TST EoS for Methane, Carbon dioxide and Nitrogen.

4. Results and discussion

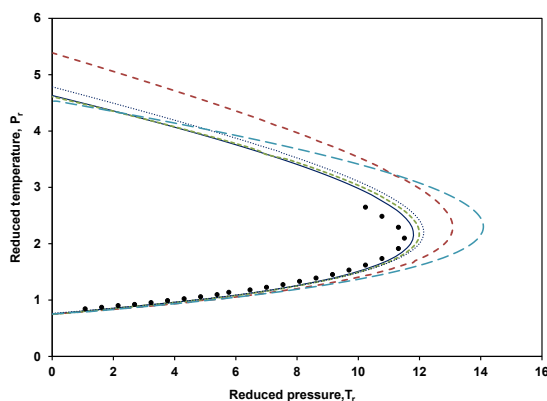
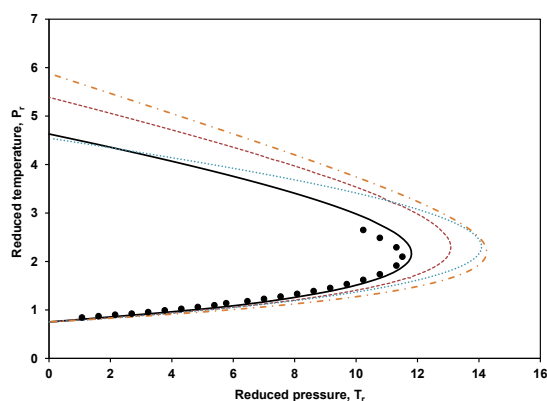
The development of high-speed computers, the established theories of statistical mechanics and the developed high accurate EoSs have made us possible the understanding the relationship of J-T coefficients and intermolecular forces. It has been observed that the prediction of J-T inversion curves by the EoSs can be made successfully by plotting the graphs between pressures and temperatures for the considered pure components and mixtures. Up to now, many forms of EoSs have been tested to find good agreement between experimental and theoretical plots of J-T inversion curves. In this work, it has been established that not only the two parameters models of EoSs such as SRK, PR etc. used till today are efficient in predicting the J-T coefficients but also three parameter models such as ER, PT and HKMM EoSs are equally efficient. Figure 1 represents the J-T inversion curves plotted from five EoSs. The calculated inversion curves have been plotted on co-ordinates of reduced pressure and reduced temperatures together to show comparison among the generated curves.

Table 5. Cohesion functions or α functions and its first derivatives used in this work are given:

EOs	Reported α functions for the EoSs	First derivatives of α functions
SRK [21]	$\alpha(T_r) = [1 + m(\omega)(1 - \sqrt{T_r})]^2$ where, $m(1 + m) \geq 0$	$\frac{d\alpha}{dT_r}(T_r) = -m(\omega)\sqrt{\frac{\alpha(T_r)}{T_r}}$, $m(\omega) = 0.480 + 1.574\omega - 0.176\omega^2$
PR [29]	$\alpha(T_r) = [1 + k(\omega)(1 - \sqrt{T_r})]^2$	$\frac{d\alpha}{dT_r}(T_r) = -k(\omega)\sqrt{\frac{\alpha(T_r)}{T_r}}$, $k(\omega) = 0.374 + 1.542\omega - 0.269\omega^2$
PT [26]	$\alpha(T_r) = [1 + F(\omega)(1 - \sqrt{T_r})]^2$	$\frac{d\alpha}{dT_r}(T_r) = -F(\omega)\sqrt{\frac{\alpha(T_r)}{T_r}}$, $F(\omega) = 0.452 + 1.309\omega - 0.295\omega^2$
ER [24]	$\alpha(T_r) = [m_1 + m_2(1 - \sqrt{T_r})]^2$ $m_1(\omega) = 0.999 - 0.010\omega - 0.008\omega^2$ $m_2(\omega) = 0.440 + 1.529\omega - 0.47\omega^2$	$\frac{d\alpha}{dT_r}(T_r) = -m_2(\omega)\sqrt{T_r\alpha(T_r)}$,
TST 1988 [32]	$\alpha(T_r) = T_r^{N(M-1)} \exp[L(1 - T_r^{NM})]$ $LM \geq 0$ $M \leq 0.8909$	$\frac{d\alpha}{dT_r}(T_r) = -\frac{\alpha(T_r)}{T_r}P(T_r)$ See Table 6 $P(T_r) = -N(M-1) + LMNT_r^{MN}$
HKMM [25]	$\alpha(T_r) = \exp[(K_4 + K_5T_r)(1 - T_r^C)]$ $C = K_6 + K_7\omega + K_8\omega^2$	$\frac{d\alpha}{dT_r}(T_r) = \alpha(T_r)[K_5 - K_4CT_r^{C-1} - K_5(C+1)T_r^C]$ $K_4 = 3.058, K_5 = 1.5479, K_6 = 0.0821, K_7 = 0.3042,$ $K_8 = -0.0730.$
Chapoy [31]	$\alpha(T_r) = \exp[C_1(1 - T_r)]$ $\times [1 + C_2(1 - T_r^{1/2})^2 + C_3(1 - T_r^{1/2})^3]^2$	$\frac{d\alpha}{dT_r}(T_r) = -C_1\alpha(T_r) + \frac{2}{\sqrt{T_r}}[\exp[C_1(1 - T_r)]\alpha(T_r)]^{1/2}$ $\times [-C_2(1 - T_r^{1/2}) - \frac{3}{2}C_3(1 - T_r^{1/2})^2]$ $C_1 = .144\omega + 1.383\omega^2 + 0.387; C_2 = -2.5214\omega^2 +$ $0.6939\omega + 0.0325; C_3 = 0.6225\omega + 0.2236$
LLS [28]	$\alpha(T_r) = T_r^{-\Theta}$	$\frac{d\alpha}{dT_r}(T_r) = -\Theta T_r^{-\Theta-1}$, $\Theta = 0.1971 + 0.0863\omega + 0.357\omega + 0.0036\omega M$ $= 0.1398(\text{Methane})$
TST 1995 [32]	$\alpha = \alpha^{(0)}(T_r) + \omega[\alpha^{(1)}(T_r) - \alpha^{(0)}(T_r)]$ $\alpha^{(0)}(T_r) = T_r^{N1(M1-1)} \exp[L1(1 - T_r^{N1M1})]$ $\alpha^{(1)}(T_r) = T_r^{N2(M2-1)} \exp[L2(1 - T_r^{N2M2})]$ For methane: L1=0.401219; M1=4.963075; N1=-0.2000. L2=0.024955; M2=1.248088; N2=-8.0000.	$\frac{d\alpha}{dT_r}(T_r) = -\frac{\alpha(T_r)}{T_r}P(T_r)$ $P(T_r) = -N(M-1) + LMNT_r^{MN}$ $\frac{d\alpha}{dT_r}(T_r) = \frac{d\alpha^{(0)}}{dT_r}(T_r) + \omega \left[\frac{d\alpha^{(1)}}{dT_r}(T_r) + \frac{d\alpha^{(0)}}{dT_r}(T_r) \right]$ $\frac{d\alpha^{(0)}}{dT_r}(T_r) = -\frac{\alpha^{(0)}}{T_r}(T_r)P^{(0)}(T_r)$ $P^{(0)}(T_r) = -N1(M1-1) + L1M1N1T_r^{M1N1}$ $\frac{d\alpha^{(1)}}{dT_r}(T_r) = -\frac{\alpha^{(1)}}{T_r}(T_r)P^{(1)}(T_r)$ $P^{(1)}(T_r) = -N2(M2-1) + L2M2N2T_r^{M2N2}$

Table 6. Representing the constants of TST EoS [32].

Compounds	L	M	N
Methane	0.0813821	0.905296	-2.13000
Carbon dioxide	0.9459510	0.888652	0.650000
Nitrogen	0.0649944	0.892385	2.34000

**Figure 1.** J-T inversion curves plotted from five different EoS namely, the PR, ER, PT, HKMM and the Chapoy with their frequently used cohesion function [24-27,29]. Solid black circles are the experimental data points for methane.**Figure 2.** J-T inversion curves plotted with the PR EoS and the Chapoy cohesion function (Dashed-line), the PR EoS and the Soave cohesion function (dash-dotted-line), the PR EoS and the TST cohesion function (dotted-line), and the ER EoS and the cohesion function associated with this EoS (solid-line). The ER EoS has been plotted for comparison [24,29,31,32]. Solid black circles are the experimental data points for methane.

In upper part of the curves the SRK EoS, PT EoS and the ER EoS are coincident. For the lower part of the curves, the HKMM EoS, PT EoS, PR EoS and the ER EoS show the trend of coincidence and are in agreement with experimental data of methane. However, the ER EoS represents the better trend among them as it shows good agreement both for lower and upper part of the curve with the other plots and experimental value of methane. Figure 2 represents the plots for J-T inversion curves by using the PR EoS with A. Chapoy [31], the Tau-Sim-Tassone [32] and the Soave cohesion functions and also with the ER EoS with its associated cohesion function $\alpha(T_r)$. The Figure 2 shows a good agreement of these plots with experimental data of methane furthermore the ER equation of state agrees more closely with the available experimentally measured data of methane than the EoS of Peng-Robinson. Figure 3 shows the inadequacy of the curve of LLS EoS. The lower part of the curve is in agreement with the experiment while the other parts are totally in disagreement.

In this work, the best prediction of J-T curve has been found by PR EoS, as none of the EoSs are able to predict the entire inversion curve accurately; however the ER EoS gives best overall prediction. Though the predictions of J-T coefficients with the considered EoS and with the associated cohesion functions are comparable with the experimental

observations but one should be very cautious in choosing the EoS as its accuracy will result a good comparison with experiment. However, it should be noted that accuracy in measuring the pressure drop in an isenthalpic experiment and interpolating data is very difficult and hence also experimentally J-T coefficient cannot be obtained with 100% accuracy. In general, the calculated low temperature part of the inversion curve is insensitive to the parameter in the equation, however, the peak of the inversion curve and the high temperature part show large variations with the eccentricity. The curve is parabolic in shape, with a maximum inversion pressure at an intermediate temperature. Within the region bounded by the J-T inversion curve, the free expansion causes a decrease in temperature. Outside the region bounded by the inversion curve more collision of molecules causes increase in temperature. The complete inversion curves of many fluids cannot be established, as they run into regions of high temperature or pressure not accessible to experimental measurements. The studied models of EoSs have a better agreement in the low temperature branch whereas noticeable differences occur in the high temperature branch for nitrogen and CO₂ both. It has been studied that by Collins *et al.* [32] that the J-T experiment are more sensitive to pressure and temperature in the high temperature branch.

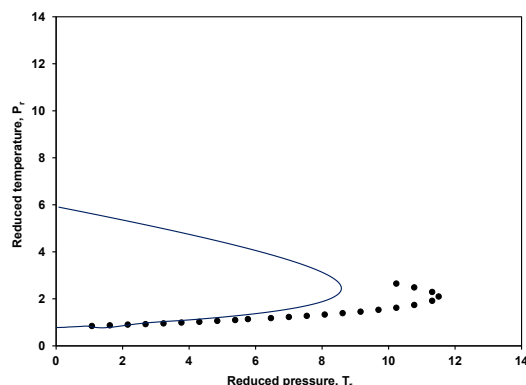


Figure 3. J-T inversion curve plotted with the LLS EoS [27] with experimental data of methane.

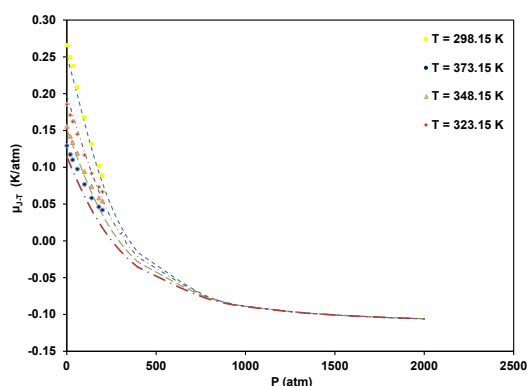


Figure 4. J-T coefficients prediction with pressure for Nitrogen at different temperatures from the PT EoS. The experimental data is taken from [33].

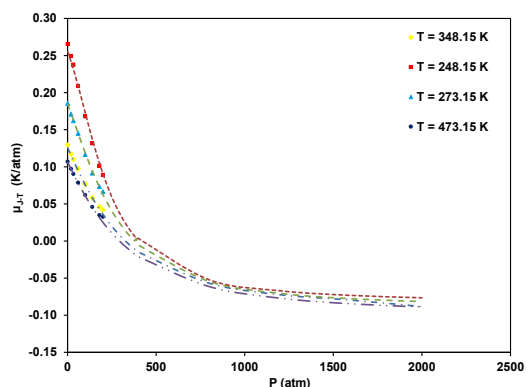


Figure 5. J-T coefficients prediction with pressure for carbon dioxide at different temperatures from the PR EoS. The experimental data is taken from [33].

In Figures 4-7, the plots for J-T coefficients against pressure at constant temperatures and in Figures 8 and 9, J-T coefficients against temperatures at constant pressure have also been performed. Because of a lack of experimental data at high pressures, all the models considered here seem to predict a negative J-T effect at 500 atm and all temperatures. In fact, it has been observed that at high pressures the J-T coefficient approaches more or less a constant for the tested components. At high pressure the negativity of J-T coefficient yields the reverse J-T effect. As the J-T coefficient is negative at high pressures, the temperature of the gas increases with the pressure drop. It is called the reverse J-T effect due to decrease in pressure with increase in temperature. A positive value of J-T coefficient corresponds to a decrease in temperature with decreasing pressure. The uncertainty of experimental J-T coefficients values from calculated EoSs of the PT, PR, HKMM,

ALU and the ER are given in Table 7 and 8. Experimental uncertainties can be observed in Figure 10.

5. Conclusions

A comprehensive comparison was made among different parameter EoSs in calculation of J-T coefficients for nitrogen and carbon-dioxide over a wide pressure and temperature ranges. The calculated result shows that the three parameter EoSs has some advantage over the two parameters cubic EoSs in calculation of J-T coefficient of pure components over a wide temperature and pressure ranges. The poorer performance of prediction of J-T coefficient was resulted by the LLS EoS and whereas the best prediction is given by the ER EoS. As regards the prediction of the J-T inversion curve, it was found a reasonable agreement among the considered models in the

Table 7. Joule-Thomson coefficient data for carbon dioxide at 1 atm and the uncertainty.

K	JT-C Expt. Data	Theoretical Joule-Thomson coefficient data from EoSs and the uncertainty, ΔU									
		ΔU	P-R EoS	ΔU	P-T EoS	ΔU	E-R EoS	ΔU	HKMM EoS	ΔU	ALU EoS
223.15	2.4130	1.8154	0.24	1.8150	0.24	1.8560	0.23	1.7897	0.25	1.8167	0.24
273.15	1.2900	1.3118	-0.17	1.3066	-0.01	1.3298	-0.03	1.3072	-0.01	1.3117	-0.01
323.15	0.8950	0.9845	-0.1	0.9765	-0.09	0.9891	-0.10	0.9984	-0.11	0.9837	-0.09
373.15	0.6490	0.7563	-0.16	0.7468	-0.15	0.7525	-0.15	0.7846	-0.20	0.7552	-0.11
398.15	0.5600	0.6669	-0.19	0.6568	-0.17	0.6601	-0.17	0.7008	-0.25	0.6657	-0.18
423.15	0.4890	0.5897	-0.20	0.5792	-0.18	0.5804	-0.18	0.6283	-0.28	0.5885	-0.20
473.15	0.3770	0.4638	-0.23	0.4528	-0.20	0.4509	-0.19	0.5095	-0.35	0.4624	-0.22
523.15	0.3075	0.3662	-0.19	0.3550	-0.15	0.3509	-0.14	0.4165	-0.35	0.3647	-0.18
573.15	0.2650	0.2889	-0.09	0.2777	-0.04	0.2721	-0.02	0.3420	-0.28	0.2874	-0.08

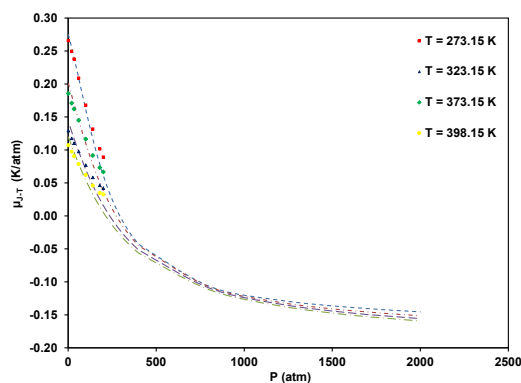
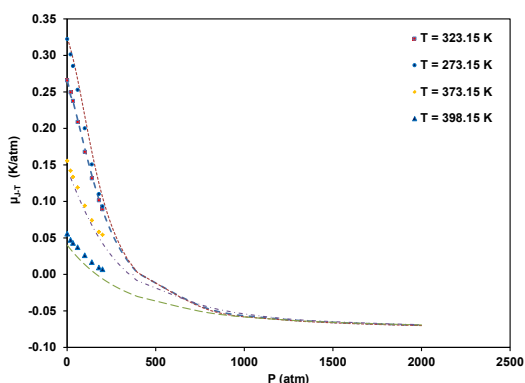
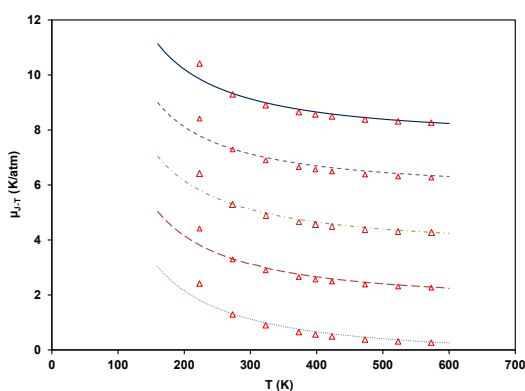
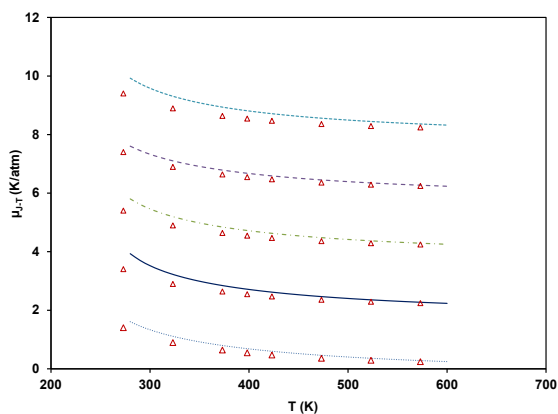
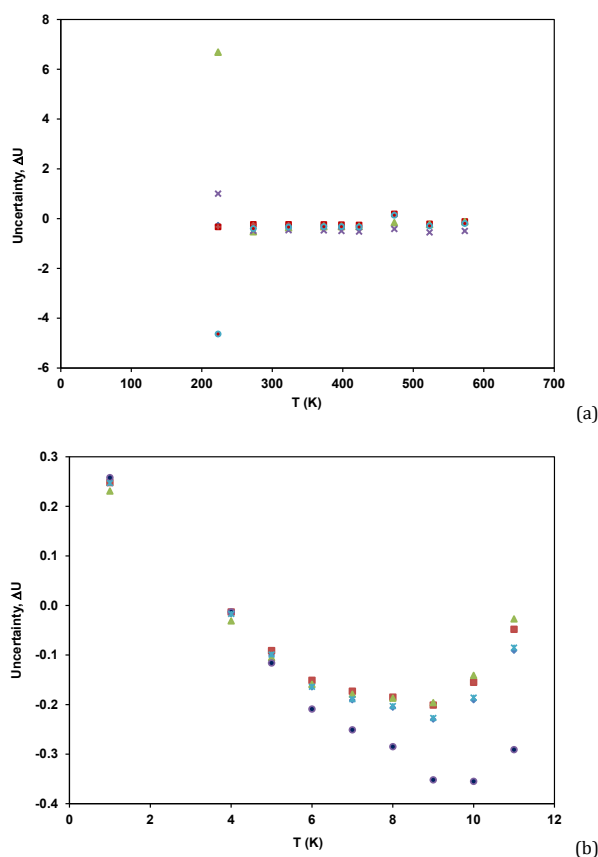
**Figure 6.** J-T coefficients prediction with pressures for carbon dioxide at different temperatures from the HKMM EoS. The experimental data is taken from [33].**Figure 7.** J-T coefficients prediction with pressures for nitrogen at different temperatures from the ER EoS. The experimental data is taken from [33].**Figure 8.** J-T coefficients ~ Temperatures graph for carbon dioxide at 1 atm plotted from different EoS. The ER EoS (Solid line), HKMM EoS (Dashed line), PT EoS (Dot-dashed line), ALS EoS (Dashing line) and the PR EoS (Dotted line). The experimental points and the lines of EoSs have been shifted upward for clear view. The experimental data is taken from [33].

Table 8. Joule-Thomson coefficient data for carbon dioxide at 20 atm and the uncertainty.

K	JT-C Expt. Data	Theoretical Joule-Thomson coefficient data from EoSs and the uncertainty, ΔU									
		ΔU	P-R EoS	ΔU	P-T EoS	ΔU	E-R EoS	ΔU	HKMM EoS	ΔU	ALU EoS
198.15	-0.020	-0.042	-1.13	-0.043	-1.17	-0.098	-3.92	-0.021	-0.07	-0.078	-2.93
223.15	-0.014	-0.017	-0.26	-0.018	-0.33	-0.107	-6.68	0.0001	1.004	-0.078	-4.63
273.15	1.4020	1.7293	-0.23	1.7270	-0.23	2.1344	-0.52	2.0821	-0.48	1.9614	-0.39
373.15	0.8950	1.1091	-0.23	1.1023	-0.23	1.2242	-0.36	1.3082	-0.46	1.1966	-0.33
323.15	0.6375	0.7959	-0.24	0.7872	-0.23	0.8431	-0.32	0.9380	-0.47	0.8425	-0.32
373.15	0.5450	0.6876	-0.26	0.6782	-0.24	0.7183	-0.31	0.8137	-0.49	0.7235	-0.32
398.15	0.4695	0.5987	-0.27	0.5889	-0.25	0.6180	-0.31	0.7131	-0.51	0.6271	-0.33
423.15	0.5575	0.4611	0.17	0.4508	-0.19	0.4659	-0.16	0.5598	-0.41	0.4796	-0.14
473.15	0.2885	0.3592	-0.24	0.3487	-0.20	0.3556	-0.23	0.4477	-0.55	0.3718	-0.28
573.15	0.2425	0.2809	-0.15	0.2703	-0.11	0.2721	-0.12	0.3620	-0.49	0.2896	-0.19

**Figure 9.** J-T coefficients ~ temperatures graph for carbon dioxide at 10 atm plotted from different EoS. The ER EoS (Solid line), HKMM EoS (Dashed line), PT EoS (Dashed line), ALS EoS (Dot-Dashed line) and the PR EoS (Dotted). The experimental points and the lines of EoSs have been shifted upward for clear view. The experimental data is taken from [33].**Figure 10.** Uncertainty in J-T coefficients or relative errors between theoretical values calculated from the EoSs of the PR, ER, HKMM and the ALS and the experimental J-T coefficients. Symbols are representing the uncertainty obtained from the EoSs at 1 atm (a) and 20 atm (b).

low-temperature branch and also the cubic EoSs yield a smaller P-T region of positive J-T coefficient. In general, for the pure components tested, the three parameters cubic EoS models seem to be superior to the two parameters cubic EoS models in calculation of derivative property such as J-T coefficient.

Acknowledgements

The authors are thankful to Dr. Satyendra Narayan Singh for useful comments and to Dr. Binita Sharan for departmental facilities.

Disclosure statement


Conflict of interests: The authors declare that they have no conflict of interest.

Author contributions: All authors contributed equally to this work.

Ethical approval: All ethical guidelines have been adhered.

ORCID

Binay Prakash Akhoury

 <http://orcid.org/0000-0003-4978-9367>

Sumit Kaur

 <http://orcid.org/0000-0003-2288-3134>

References

- [1]. Roebuck, J. R.; Osterberg, H. *Physic. Rev.* **1935**, *48*, 450-457.
- [2]. Sage, B. H. *Soc. Petrol. Engin.* **1943**, *151*, 1-9.
- [3]. Kenneth, J. K.; Wenzel, L. A. *AIChE Jour.* **1972**, *18*, 684-688.
- [4]. Adachi, Y.; Benjamin, C.; Lu, Y.; Sugie, H. *Fluid Phase Equilib.* **1983**, *11*, 29-48.
- [5]. Matin, N. S.; Haghighi, H. *Fluid Phase Equilib.* **2000**, *175*, 273-284.
- [6]. Vrabc, J.; Kumar, A.; Hasse, H. *Fluid Phase Equilib.* **2009**, *258*, 34-40.
- [7]. Chacin, A.; Vazquez, J. M.; Muller, E. A. *Fluid Phase Equilib.* **1999**, *165*, 147-155.
- [8]. Rde Groot, S.; Michels, A. *Physica.* **1948**, *14*, 218-222.
- [9]. Matin, N. S. *J. Chem. Engin. Japan* **1997**, *30*, 520-525.
- [10]. Abbas, R.; Ihmel, C.; Enders, S.; Gmehling, J. *Fuel Energy* **2011**, *30*, 181-189.
- [11]. Prausnitz, J. M.; Gunn, R. D.; Chueh, P. L. *Cryogen* **1966**, *6*, 324-329.
- [12]. Potter, J. H. *J. Eng. Indust.* **1970**, *92*, 257-262.
- [13]. Nichita, D. V.; Leibovici, C. *Fluid Phase Equilib.* **2006**, *246*, 167-176.
- [14]. Coleman, T. C.; Stewart, R. B., Presented at the NAS-NRC 13th International Congress of Refrigeration, Washington, DC, 1971.
- [15]. Bender, E., Proceedings of the Fifth Symposium on Thermophysic. Propert. ASME, 1970, pp. 227-235.
- [16]. Brown, E. H.; Dean, J. W. *J. Res. Nation Burea Stand.* **1958**, *60*, 161-168.
- [17]. Miller, D. G. *Ind. Eng. Chem. Fund.* **1970**, *9*, 585-589.
- [18]. Deiters, U. K.; DeReuck, K. M. *Pure Appl. Chem.* **1997**, *69*, 1237-1249.
- [19]. Nasrifar, K.; Bolland, O. *Ind. Eng. Chem. Res.* **2004**, *43*, 6901-6909.
- [20]. Soave, G. *Chem. Eng. Scie.* **1972**, *27*, 1197-1203.
- [21]. Redlich, O.; Kwong, J. N. S. *Chem. Rev.* **1949**, *44*, 233-244.
- [22]. Dilay, G. W.; Heidemann, R. A. *Ind. Engin. Chem. Fund.* **1986**, *25* 152-158.
- [23]. Colina, C. M.; Lisal, M.; Siperstein, F. R.; Gubbins, K. E. *Fluid Phase Equilib.* **2002**, *202*, 253-262.
- [24]. Esmaeilzadeh, F.; Roshanfekar, M. *Fluid Phase Equilib.* **2006**, *293*, 83-90.
- [25]. Haghtalab, A.; Kamali, M. J.; Mazloumi, S. H.; Mahmoodi, P. *Fluid Phase Equilib.* **2010**, *293*, 209-218.
- [26]. Teja, A. S.; Patel, N. C. *Chem. Eng. Scie.* **1982**, *37*, 463-473.
- [27]. Adachi, Y.; Sugie, H.; Nakanishi, K.; Lu B. C. *Fluid Phase Equilib.* **1989**, *52*, 83-90.
- [28]. Lawal, A. S.; Silberberg, I. H. *Soc. Pet. Eng.* **1985**, *1*, 1-21.
- [29]. Peng, D. Y.; Robinson, D. B. *Ind. Eng. Chem. Fund.* **1976**, *15*, 59-64.
- [30]. Taylor, H. S.; Gasstone, S., A treatise on Physical Chemistry, 3rd edition, D. Van Nostrand Company, Inc, New York 18, New York, 1924.
- [31]. Coquelet, C.; Chapoy, A.; Richon, D. *Intern. J. Thermophys.* **2004**, *25(1)*, 133-158.
- [32]. Twu, C. H.; Sim, W. D. Tassone, V. *Fluid Phase Equilib.* **2002**, *194*, 385-399.
- [33]. Green, D. W.; Perry, R. H., Perry chemical engineering handbook, McGraw-Hill, New York United States, 7th edition, 1934.



Copyright © 2019 by Authors. This work is published and licensed by Atlanta Publishing House LLC, Atlanta, GA, USA. The full terms of this license are available at <http://www.eurjchem.com/index.php/eurjchem/pages/view/terms> and incorporate the Creative Commons Attribution-Non Commercial (CC BY NC) (International, v4.0) License (<http://creativecommons.org/licenses/by-nc/4.0>). By accessing the work, you hereby accept the Terms. This is an open access article distributed under the terms and conditions of the CC BY NC License, which permits unrestricted non-commercial use, distribution, and reproduction in any medium, provided the original work is properly cited without any further permission from Atlanta Publishing House LLC (European Journal of Chemistry). No use, distribution or reproduction is permitted which does not comply with these terms. Permissions for commercial use of this work beyond the scope of the License (<http://www.eurjchem.com/index.php/eurjchem/pages/view/terms>) are administered by Atlanta Publishing House LLC (European Journal of Chemistry).